Escola de Primavera de Transição e Turbulência
Blumenau 2022

ABCM Associação Brasileira de Engenharia e Ciências Mecânicas

13th Spring School on Transition and Turbulence
September 19th-23rd, 2022, Blumenau, SC, Brazil

EPTT-2022-0020
FLUID-STRUCTURE INTERACTION FOR TURBULENT INCOMPRESSIBLE FLOW OVER A CYLINDER-PLATE SYSTEM

Freddy Alejandro Portillo Morales
Aristeu da Silveira Neto
Aldemir Aparecido Cavallini Jr.
Ricardo Tadeu Oliveira Catta Preta
Vinícius Hagemeyer Chiumento
Federal University of Uberlandia - Av. Joao Naves de Avila, 2121. Uberlandia, MG, Brasil
alejandro@ufu.br
aristeus@ufu.br
aacjunior@ufu.br
ricardocatta@gmail.com
vini.hagemeyer@gmail.com

Abstract. *For computational numerical simulations of fluid-structure interaction it is possible to use a partitioned approach, which allows separating the system into two subsystems, fluid and structural. MFSim is a multi-physics software, developed at the Fluid Mechanics Laboratory (MFLab) of the Federal University of Uberlândia, it allows to solve fluid-structure iteration problems in a partitioned way, discretizing each subsystem with a different mesh, solving them separately and communicating them at each time step. In MFSim the fluid subsystem is solved using the finite volume method (FVM) and the structural subsystem using the finite element method (FEM). As a bridge between these two methods is the immersed boundary method (IB) to calculate the fluid-dynamic forces exerted by the flow under the structure. In this work the computational simulation of FSI is solved with weak coupling (one way). The case study of this work is based on a typical validation case for FSI problems proposed by Turek and Hron (2006), it is an incompressible turbulent flow in a channel around a solid structure with an elastic part. In the structural subsystem, a mesh formed by solid hexa-8 elements with extra shape functions is used. For the fluid formulation, the Smagorinsky model is used, for turbulence closure. The results obtained are preliminary because the simulation is still in progress. Up to the time of publication, the structure has shown almost 5 mm of maximum displacement, turbulent structures are visible even though the simulation is in the stage of transition to turbulence.*

Keywords: *Fluid-structure interaction, Vibration response, Incompatible modes.*

1. INTRODUCTION

In this paper, a thin flexible structure coupled to a rigid cylinder is subjected to an incompressible flow of water in a turbulent regime. Fluid-structure interaction (FSI) cases with simple geometries are useful in validating results when compared with experimental results. Through numerical simulation it is possible to observe the behavior of the system changing the different parameters that influence the physical model. The simulations performed in this work were executed in the (in-house) program MFSim. MFSim is a multiphysics numerical simulation program that allows solving problems of compressible and incompressible flows, as well as fluid structure interaction, multiphase flows and combustion. In MFSim a discretized Eulerian domain with a block-structured mesh is used and solved by the Finite Volume Method (FVM), for the Lagrangian domain it is possible to be discretized with beam, plate, shell and solid elements and this is solved through the Finite Element Method (FEM), for the FSI to happen an interface is needed, which is the Immersed Boundary (IB), which is composed of a mesh of .STL format (StereoLithography) and through the use of the Immersed Boundary Method (IBM) and Multi-Direct Forcing (MDF) it is possible to transfer the hydrodynamic forces that the flow exerts under the IB to the structure at each time step. For this case, we used the LES methodology to model the turbulence closure. We apply the Smagorinsky model, developed by Smagorinsky (1963).

2. TUREK-HRON PROBLEM SPECIFICATION

This work is based on the comparative evaluation carried out by Turek and Hron (2006), which consists in the analysis of fluid-structure interaction of a cylinder-plate system subjected to an incompressible flow of water in a laminar regime.

For the specific case under study, an incompressible flow of water in a turbulent regime was used, with Re = 110 000. In Figure 1 an illustration of the physical model adopted for the numerical simulations is shown, the dimensions of the geometrical configuration, from Wu, are arranged in Table 1. The Table 2 shows the mechanical properties for each material used. In Figure 2 the fluid and structure domains used are shown.

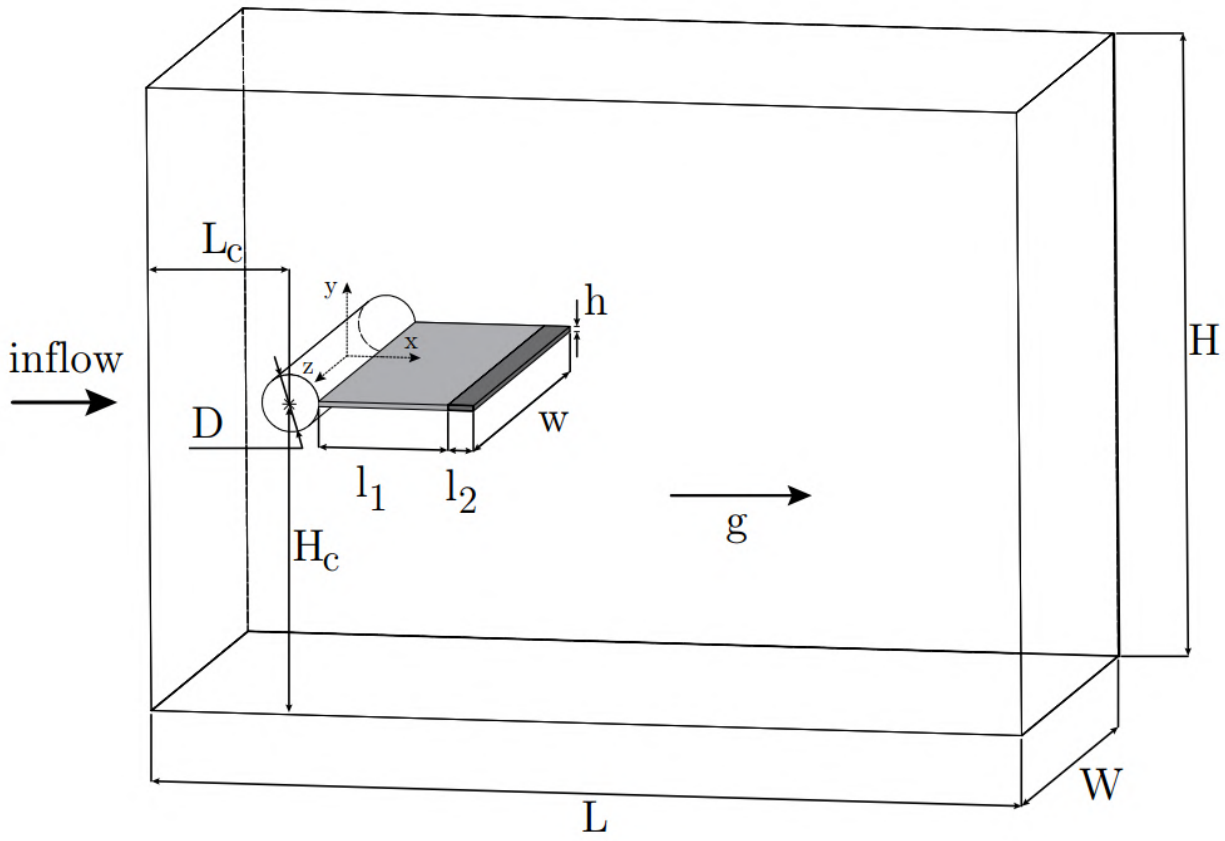

Figure 1. Physical model and dimensions for fluid and structure domains (Nayer and Breuer, 2014)

Table 1. Geometrical configuration

Concept	**value (m)**
Cylinder diameter	$D = 0.022$
Cylinder center x-position	$L_c = 0.077$
Cylinder center y-position	$H_c = 0.120$
Test section length	$L = 0.480$
Test section height	$H = 0.240$
Test section width	$W = 0.180$
Deformable structure length	$l_1 = 0.050$
Deformable structure height	$h = 0.002$
Deformable structure width	$w = 0.177$
Steel mass length	$l_2 = 0.010$
Steel mass height	$h = 0.002$
Steel mass width	$w = 0.177$

Table 2. Structural properties

Para-rubber	
Density	$\rho_r = 1090\, kg/m^3$
Young's modulus	$E_r = 4.1\, MPa$
Poisson's ratio	$\nu_r = 0.48$
Steel	
Density	$\rho_s = 7850\, kg/m^3$
Young's modulus	$E_s = 210 \times 10^3\, MPa$
Poisson's ratio	$\nu_s = 0.3$

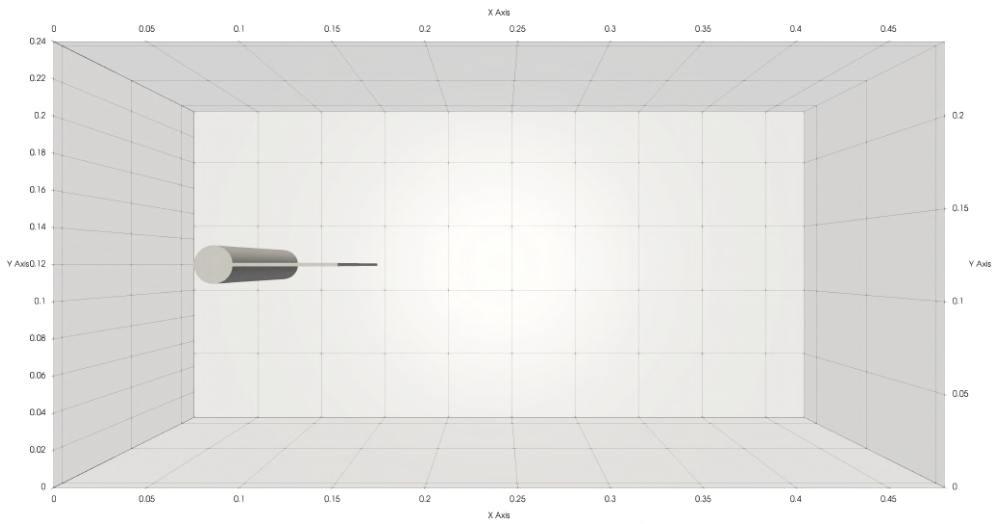

Figure 2. Fluid and structure domains for numerical simulations

3. DIFFERENTIAL MODEL

This case studies a Newtonian incompressible flow that interacts with an elastic solid. The solved balance equations for the fluid subsystem are the continuity equation (Eq. 1) and conservation of linear momentum equation (Eq. 2).

$$\frac{\partial u_i}{\partial x_i} = 0, \quad i = 1, 2, 3 \tag{1}$$

$$\frac{\partial u_i}{\partial t} + \frac{\partial (u_i\, u_j)}{\partial x_j} = -\frac{1}{\rho_f}\frac{\partial P}{\partial x_i} + \frac{\partial}{\partial x_j}\left[\nu\left(\frac{\partial u_i}{\partial x_j} + \frac{\partial u_j}{\partial x_i}\right)\right] + f_i \tag{2}$$

Where i and $j = 1, 2, 3$, P is the pressure, t is the time variable and f_i is the external forces. For the structure subsystem, the equations of motion are solved (Eq. 3).

$$[M]\{\ddot{x}\} + [C]\{\dot{x}(t)\} + [K]\{x(t)\} = f(t) \tag{3}$$

where $[M]$, $[K]$ and $[C]$ are the mass, stiffness and damping matrices. $\ddot{x}$, $\dot{x}$ and x are the acceleration, velocity and displacement vectors and $f(t)$ are the external forces.

4. MATHEMATICAL MODEL

4.1 FEM: 8-node hexahedron with extra shape functions

For the structural model, the 8-node hexahedral solid element with extra shape functions was used. This element type adds a quadratic term in three directions to the standard 8-node hexahedral element shape functions. The shape functions are as follows:

$$x = \sum_{i=1}^{8} N_i(\xi,\eta,\zeta)x_i + [P]\{\alpha\}, \quad y = \sum_{i=1}^{8} N_i(\xi,\eta,\zeta)y_i + [P]\{\alpha\}, \quad z = \sum_{i=1}^{8} N_i(\xi,\eta,\zeta)z_i + [P]\{\alpha\} \tag{4}$$

Where $[P]\{\}$ are the quadratic terms added as incompatible modes.

The calculation of the elementary stiffness matrix is performed using Eq. 5. With the addition of the incompatible modes the stiffness matrix calculation is now calculated with Eq. 6. The stiffness matrix is then subdivided into four submatrices (K_{aa},$K_{a\alpha}$,$K_{\alpha a}$ and $K_{\alpha\alpha}$). In Eq. 8 the elementary equilibrium equation is shown in Morales (2021).

$$[K_e] = \iiint_{V_e} [B]^T[D][B]dV_e \tag{5}$$

$$[K_e] = \iiint_{V_e} \begin{bmatrix}[B_a]^T \\ [P']^T\end{bmatrix} \Big[D\Big] \begin{bmatrix}[B_a] & [P']\end{bmatrix} dV_e \tag{6}$$

$$[K_e] = \iiint_{V_e} \begin{bmatrix}\Big[[B_a]^T[D][B_a]\Big] & \Big[[B_a]^T[D][P']\Big] \\ \Big[[P']^T[D][B_a]\Big] & \Big[[P']^T[D][P']\Big]\end{bmatrix} dV_e \tag{7}$$

$$\begin{bmatrix}[K_{aa}]_{24x24} & [K_{a\alpha}]_{24x9} \\ [K_{\alpha a}]_{9x24} & [K_{\alpha\alpha}]_{9x9}\end{bmatrix} \begin{Bmatrix}\{d_a\}_{24x1} \\ \{\alpha\}_{9x1}\end{Bmatrix} = \begin{Bmatrix}\{F_a\}_{24x1} \\ \{0\}_{9x1}\end{Bmatrix} \tag{8}$$

To remove non-nodal displacements (α) static condensation is used, which is derived in Eq. 9. The way to obtain the stiffness submatrices can be found in Morales (2021).

$$\Big[[K_{\alpha\alpha}] - [K_{a\alpha}][K_{\alpha\alpha}]^{-1}[K_{\alpha a}]\Big] d_a = F_a \tag{9}$$

Therefore, the condensed elementary stiffness matrix to be used by the incompatible element theory is shown in Eq. 10.

$$[K_e] = \iiint_{V_e} \left[\Big[[B_a]^T[D][B_a]\Big] - \Big[[B_a]^T[D][P']\Big]\Big[[P']^T[D][P']\Big]^{-1}\Big[[P']^T[D][B_a]\Big]\right] dV_e \tag{10}$$

The elementary mass matrix is calculated with Eq. 11.

$$[M_e] = \iiint_{V_e} \rho[N]^T[N]\, dV_e \tag{11}$$

Transforming the Eq. 10 and 11 to the isoparametric coordinate system (ξ,η,ζ) obtains the Eq. 12 and 13.

$$[K_e] = \int_{-1}^{+1}\int_{-1}^{+1}\int_{-1}^{+1} \left[\Big[[B_a]^T[D][B_a]\Big] - \Big[[B_a]^T[D][P']\Big]\Big[[P']^T[D][P']\Big]^{-1}\Big[[P']^T[D][B_a]\Big]\right] det[\mathbf{J}]\, d\xi\, d\eta\, d\zeta \tag{12}$$

$$[M_e] = \int_{-1}^{+1}\int_{-1}^{+1}\int_{-1}^{+1} \rho[N]^T[N] det[\mathbf{J}]\, d\xi\, d\eta\, d\zeta \tag{13}$$

The solutions for Eq. 12 and 13 can be obtained through the use of numerical Gauss integration, which for an element of 8 nodes, two integration points would be sufficient. The three-dimensional Gauss numerical integration is shown in Eq. 14.

$$I = \int_{-1}^{+1}\int_{-1}^{+1}\int_{-1}^{+1} f(\xi,\eta,\zeta)d\xi d\eta d\zeta = \sum_{i=1}^{n}\sum_{j=1}^{m}\sum_{k=1}^{l} = w_i w_j w_k f(\xi_i,\eta_j,\zeta_k), \tag{14}$$

where, w_i, w_j and w_k are the weight functions that depend on the number of quadrature points and f is the function in the isoparametric natural coordinates.

4.2 Turbulence model

The Reynolds number of the analyzed problem is quite high. Consequently, the number of degrees of freedom of the problem generates an impractical computational cost — if it is solved with Direct Numerical Simulation. Therefore, we decided to address the problem using the LES methodology. To model turbulence, we need to apply low-pass filtering on Eq. 2. We know that the velocity field can be decomposed into two parts. A filtered part ($\bar{u}_i$) and a floating part ($u^{'}$). Substituting $u_i = \bar{u}_i + u^{'}$ into Eq. 2, we get

$$\frac{\partial \bar{u}_i}{\partial t} + \frac{\partial (\bar{u}_i\, \bar{u}_i)}{\partial x_j} = -\frac{1}{\rho_f}\frac{\partial \bar{p}}{\partial x_i} + \frac{\partial}{\partial x_j}\left[\nu\left(\frac{\partial \bar{u}_i}{\partial x_j} + \frac{\partial \bar{u}_j}{\partial x_i}\right)\right] + \frac{f_i}{\rho_f} + \frac{\partial \tau_{ij}}{\partial x_j}, \tag{15}$$

where $\tau_{ij} = \bar{u}_i\bar{u}_j - \overline{\bar{u}_i\bar{u}_j}$ is the components of sub-grig tensor.

To solve the τ_{ij} closure problem, we use the Smagorinsky model, where $\tau_{ij} = 2\nu_t\bar{S}_{ij}$, $\nu_t = (Cs\Delta)^2(\bar{S}_{ij}\bar{S}_{ij})^{1/2}$ and $\bar{S}_{ij} = \frac{1}{2}\left(\frac{\partial \bar{u}_i}{\partial x_j} + \frac{\partial \bar{u}_j}{\partial x_i}\right)$. We use the value of the Smagorinsky constant as Cs = 0.25. Substituting the previous relationships in Eq. 15, we arrive at the following equation for turbulence closure:

$$\frac{\partial \bar{u}_i}{\partial t} + \frac{\partial (\bar{u}_i\, \bar{u}_i)}{\partial x_j} = -\frac{1}{\rho_f}\frac{\partial \bar{p}}{\partial x_i} + \frac{\partial}{\partial x_j}\left[\nu_{ef}\left(\frac{\partial \bar{u}_i}{\partial x_j} + \frac{\partial \bar{u}_j}{\partial x_i}\right)\right] + \frac{f_i}{\rho_f}, \tag{16}$$

where $\nu_{ef} = \nu + \nu_t$.

4.3 Immersed boundary method

The Immersed Boundary Method (*Immersed Boundary Method - IB*) emerged as an efficient alternative to methods whose meshes fit the boundaries for the treatment of problems involving complex, mobile and deformable geometries (Andrade, 2015).

This method can communicate the fluid and structure subsystems, the first of these, fluid, is an Eulerian domain and the structure subsystem is a Lagrangian domain. The immersed boundary method manages to couple these through the source term of the linear momentum balance equation, that is, the fluid dynamic forces, which after being calculated enter the Langrangian domain of the structure subsystem as external forces.

To take into account the presence of the immersed boundary, it is necessary to replace the source term $f_i\,[Nm^{-3}]$ into the filtered Navier-Stokes equations in Eq. 16 by:

$$f_i(\vec{x}) = \int_\Omega (F_k)_i(\vec{x}_k)\delta(\vec{x} - \vec{x}_k)d\vec{x}_k \tag{17}$$

where $\delta(\vec{x} - \vec{x}_k)$ is the Dirac delta function, $\vec{x}_k$ is the position of the Lagrangian point and $\vec{x}$ is the position of the Eulerian point under analysis.

5. SIMULATION SETUP

Next in the Table 3 is the configuration used in the numerical simulations performed.

Table 3. Numerical simulation setup

Parameter	
Processors reference	AMD Epyc 7452
Total number of cores	64
Total number of nodes	2
Number of fluid cells	17028932
Number of .stl elements for IB	339974
Number of Hexa8 elements for structure subsystem	5400
Number of DOFs on structure subsystem	25389
Number of modes calculated	20
Number of cells on bottom level	$80 \times 40 \times 40$
Number of refinement levels	5
Pressure-velocity coupling method	SBDF
Advective model	cubista
Turbulence closure model	Smagorinsky
Smagorinsky constant value	0.25
Cores distribution	$8 \times 2 \times 4$
Inlet flow velocity	$5\,m/s$
Physical time simulated	$4s$

The boundary conditions imposed on the Eulerian domain are:

- Dirichlet for u, v and w velocities and Neumann for pressure on the inlet face (x-).
- Advective for u, v and w velocities and Dirichlet for pressure on the output face (x+).
- Neumann for the u, v and w velocities, Dirichlet for the pressure and no-slip condition on the north (y+), south (y-), top (z+) and bottom (z-) faces.

6. RESULTS AND DISCUSSION

In Table 4 the twenty first modes of vibration are shown. For the numerical tests, 4.00 physical seconds were simulated. Figure 3 shows the velocity magnitude field, it is possible to visualize the eddy structures formation due to the flow interaction with the structure. Figure 4 shows the contours of the isoQ parameter, colored based on the magnitude of the velocity. In Figure 6 adaptive mesh based on IB movement is shown, it's composed by 5 levels of refinement.

Table 4. Vibration modes for plate

Vibrating Mode	**Frequency [Hz]**
1	3.03
2	6.97
3	32.22
4	61.29
5	61.41
6	67.19
7	75.60
8	77.32
9	87.97
10	96.44
11	104.39
12	124.84
13	149.63
14	160.92
15	161.66
16	161.66
17	161.91
18	170.71
19	178.61
20	179.82

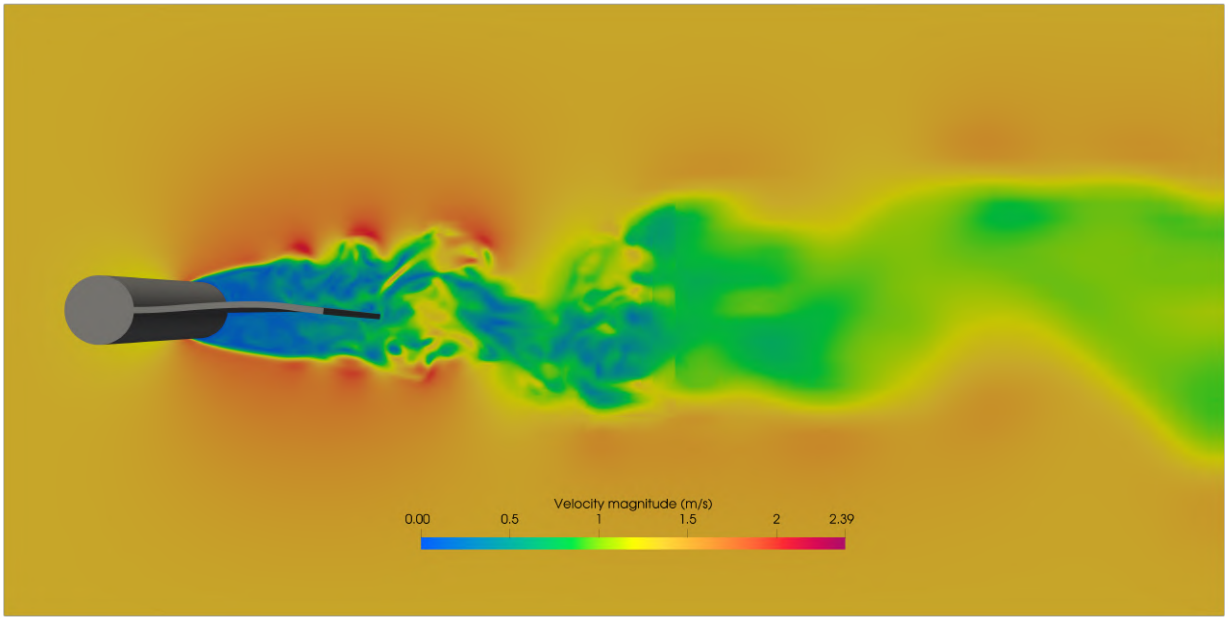

Figure 3. Velocity magnitude in m/s after 4.0 physical seconds

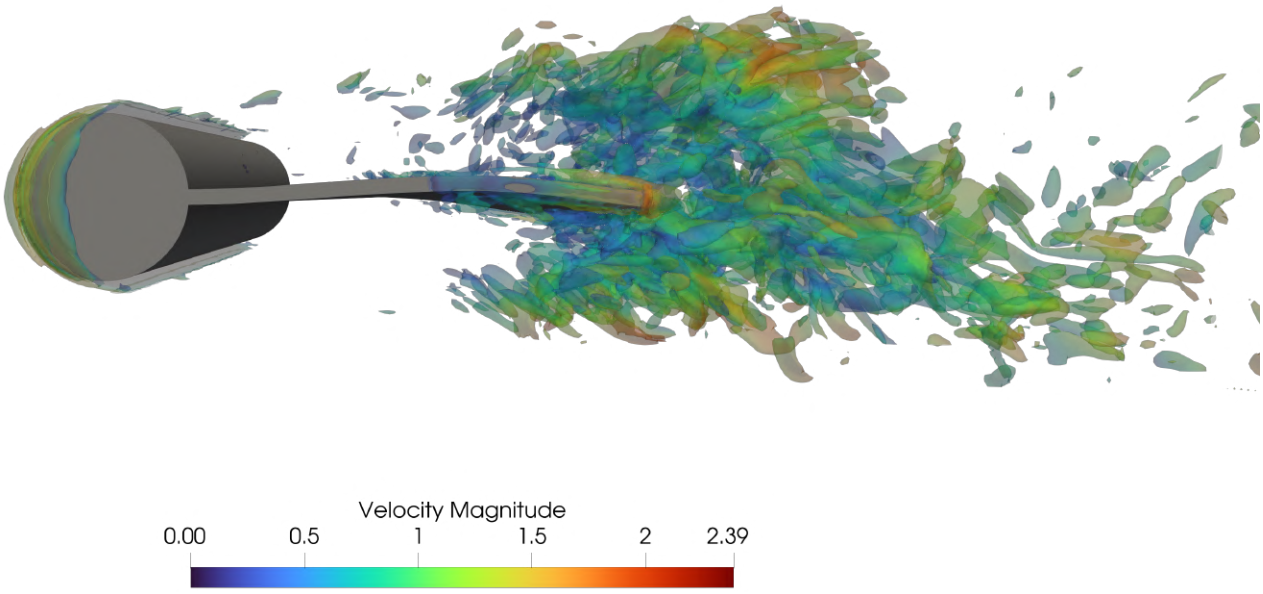

Figure 4. Contour of IsoQ after 4.0 physical seconds

Figure 5 shows the displacement of the structure due to iteration with the flow, increases in displacements are expected, probes are used to extract the nodal displacements at each time step. The vibration signals extracted from these probes will be treated using FFT (*Fast Fourier Transform*) and compared with experimental results obtained by Turek and Hron (2006) and Nayer and Breuer (2014).

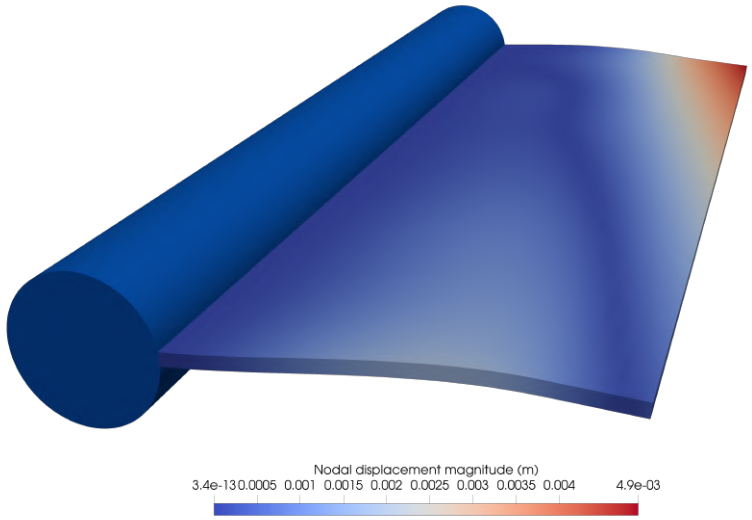

Figure 5. Structure displacement magnitude in meters (m) after 4.0 physical seconds

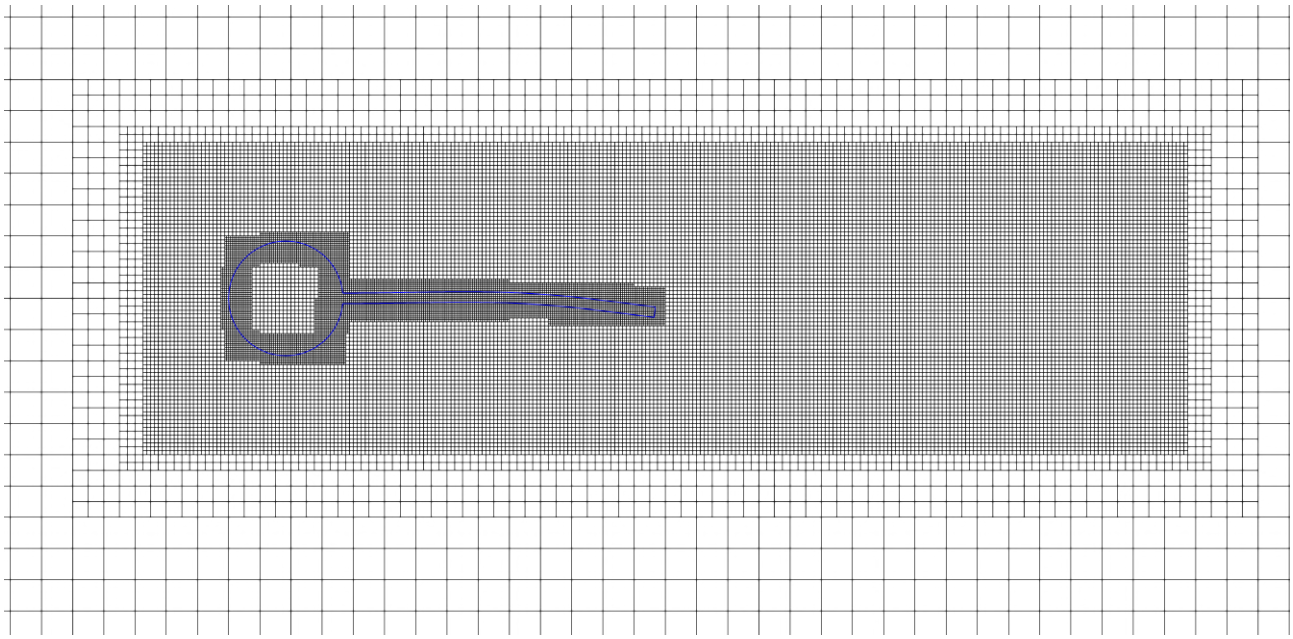

Figure 6. adaptive mesh based on IB movement

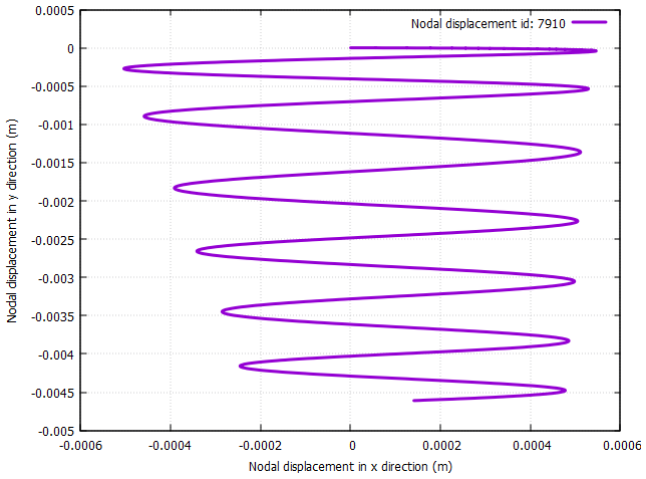

Figure 7. Nodal displacement in x direction vs nodal displacement in y direction after 4.0 physical seconds

In Figure 7 nodal displacement x vs y are shown after 4.0 physical seconds of simulation.

7. CONCLUSIONS

The results presented above are preliminary as the simulation is still in progress and is part of the validation stage of fluid-structure interaction for turbulent flows using the Smagorinsky model for turbulence closure. However, with these preliminary results, it is possible to see the creation of eddy structures due to the movement of the flexible structure (cylinder-plate system). The results obtained so far indicate the need to use an adaptive mesh based on vorticity to avoid dissipation of eddy structures. The structure presents a behavior in accordance with the expected, although the results obtained so far indicate that it is in the transition stage to turbulent flow. The use of white noise can be viable to accelerate the transition process to turbulence.

8. ACKNOWLEDGEMENTS

The authors would like to thank MFLAB, FEMEC/UFU, Petrobras, CNPq, CAPES, FURNAS Centrais Elétricas and the “Programa de Pesquisa e Desenvolvimento Tecnológico” (P&D) of the ANEEL for the financial support.

9. REFERENCES

Andrade, J.R., 2015. “Métodos de fronteira imersa para corpos esbeltos: implementação e validação”. p. 133.

Morales, F., 2021. “Fluid-structure interaction for cantilever plates immersed in air and water using solid element in structure subsystem on mfsim (in-house software)”. *COBEM: 26th International Congress of Mechanical Engineering*. doi:10.26678/ABCM.COBEM2021.COB2021-1413.

Nayer, G.D. and Breuer, M., 2014. “Numerical fsi investigation based on les: Flow past a cylinder with a flexible splitter plate involving large deformations (fsi-pfs-2a)”. *International Journal of Heat and Fluid Flow*, Vol. 50, pp. 300–315. ISSN 0142727X. doi:10.1016/j.ijheatfluidflow.2014.08.013.

Smagorinsky, J., 1963. “General circulation experiments with the primitive equations i: The basic experiment”. doi: 10.1175/1520-0493(1963)091<0099:GCEWTP>2.3.CO;2.

Turek, S. and Hron, J., 2006. “Proposal for numerical benchmarking of fluid-structure interaction between an elastic object and laminar incompressible flow”. *Lecture Notes in Computational Science and Engineering*, Vol. 53, pp. 371–385. ISSN 14397358. doi:10.1007/3-540-34596-5_15.

10. RESPONSIBILITY NOTICE

The authors are the only responsible for the printed material included in this paper.